Hindawi
Advances in Condensed Matter Physics
Volume 2021, Article ID 5422065, 8 pages
https://doi.org/10.1155/2021/5422065

Research Article

First-Principles Investigation of Structural, Electronic, and Room Temperature Ferromagnetism in Si-Doped Monolayer BN

Ahemedin Abedea Ajaybu and Sintayehu Mekonnen Hailemariam

Arba Minch University, Department of Physics, Arba Minch, Ethiopia

Correspondence should be addressed to Sintayehu Mekonnen Hailemariam; hailemariamsintayeh@gmail.com

Received 15 June 2021; Revised 16 October 2021; Accepted 11 November 2021; Published 30 November 2021

Academic Editor: Jiandi Zhang

We performed spin-polarized density functional theory (DFT) to investigate the structural, electronic, and magnetic properties of silicon- (Si-) doped monolayer boron nitride (BN). The present study revealed that structural parameters like bond length, bond angle, and lattice parameters increase as Si-doped in the B site of monolayer BN. However, the bandgap of monolayer BN is reduced in the presence of the Si dopant. Moreover, the obtained magnetic moment and analysis of the total density of states (TDOS) show that Si-doped monolayer BN displays ferromagnetism. The calculated ferromagnetic transition temperature (Tc) value for Si concentration of 12.5% is 476 K which exceeds room temperature. The findings are avenues to enhance the application of monolayer BN for spintronics.

1. Introduction

Two-dimensional materials (2D) have become a focus of research for scientists in the field of material sciences since the first successful exfoliation of single-layer graphene, owing particularly to the prospect of taking advantage of their exceptional electronic properties in novel devices [1]. Among the family of 2D materials, multilayered boron nitride (BN) compounds have received the attention of researchers [2] due to its exceptional mechanical [3], optical [4], catalytic [5], and thermal [6] properties. Especially, in the monolayer limit, its structural properties are closely related to hexagonal graphene [7]. As different theoretical and experimental results indicate BN can exist in different crystal structures, namely, hexagonal boron nitride (h-BN) [8], rhombohedral boron nitride (r-BN) [9], cubic boron nitride (c-BN) [10], and wurtzite [11]. Monolayer BN is comprised of alternating boron and nitrogen atoms in a honeycomb arrangement, consisting of sp^2-bonded two-dimensional (2D) layers [12, 13]. Within each layer of hexagonal BN, boron and nitrogen atoms are bound by strong covalent bonds, whereas the layers are held together by weak Van der Waals forces as in graphite. It has been reported the bond length of h-BN 1.451 Å is closer with graphene with bond length 1.425 Å [14].

The other attractive aspect of graphene is its semimetallic nature where the valence and conduction bands meet each other at the Dirac point [15]. Unlike zero bandgaps metallic graphene, intrinsic BN is an insulator with a direct wide bandgap [16]. The main challenges to the practical application of pristine or undoped BN is primarily its wide bandgap nature. The DFT calculation like local density approximation (LDA) estimated the bandgap of single layer BN to be 4.7 ev [17], which is less than that from calculations obtained by using Green function and the screened Coulomb interaction approximation (GWA) (5.95 eV) [18] and experimentally reported optical bandgap (5.5 eV) [19]. However, there are different theoretical and experimental evidence on the possibility of controlling the bandgap of h-BN. Among those, Wang et al. reported that the bandgap of BN can be modulated by doping with semiconductor like C [20]. In addition, recent DFT studies have shown that the bandgap of undoped h-BN can be reduced from 5.97 to 4.1 Å with 12.5% AL-doping [21]. Furthermore, Yue et al. have reported significant bandgap reduction of pristine h-BN by Si-doping [22].

The other drawback of BN for the material application is related to its paramagnetic nature in pure state [23]. For information storage and spintronics (using a spin degree of freedom for electronics), ferromagnetic ordering at a certain finite temperature is essential. Yuan and coworkers demonstrated that the doping of transition metal in h-BN sheet can alter the magnetic properties of pristine BN [24]. Moreover, Zhou et al. found that nonmagnetic semiconductor like Si doping on semiconductor G induces ferromagnetism [25]. Furthermore, more recently, it has been reported that semiconductor silicon- (Si-) doping can alter the electronic properties of monolayer BN by reducing the band gap [26, 27]. However, the detailed investigation of how structural, electronic, and magnetic properties of pristine hexagonal monolayer BN can be altered in the presence of Si substitution doping is not yet studied.

In the present study, the structural, electronic, and magnetic properties of Si-doped hexagonal BN are studied in detail using spin-polarized DFT. For the first time, we have proposed room temperature ferromagnetic transition temperature in Si-doped monolayer hexagonal BN. Our results will bring a step forward to modulate structural, electronic, and magnetic properties of a wide bandgap semiconductor (insulator) by doping another semiconductor which is relatively closer in atomic size to the mother compound.

2. Computational Details

First-principles calculations were performed based on spin-polarized DFT using the Quantum Espresso code [28]. The generalized gradient approximation of the Perdew–Burke–Ernzerhof (PBE-GGA) was the formula used for the electronic exchange-correlation potential [29]. The plane-wave basis set with a cutoff energy of 20 Ry and 60 Ry for structural relaxation and calculation, respectively, was used after performing the convergence test. To investigate the doping effects of Si impurities on monolayer BN, the BN was modeled by a supercell of $(4 \times 4 \times 1)$, as shown in Figure 1. A vacuum region of 15 Å was set along the Z-axis to avoid any interaction along the z-axis. Integrations over the Brillouin zone (BZ) were sampled based on a Monkhorst–Pack 2D grid [30]. The atomic positions were optimized until the force acting on each atom becomes less than 0.05 eV/Å. Boron (B) [He] $2s^2 2p^1$, nitrogen (N) [He] $2s^2 2p^3$, and silicon (Si) [Ne] $3s^2 3p^2$ valence electrons were considered for the simulation.

3. Result and Discussion

3.1. Effect of Si-Doping on Structural Properties of Pure Monolayer BN. After structural optimization, the calculated lattice constant is 2.512 Å. However, after the substitution of a single Si atom, the lattice constant is 2.582 Å. The calculated Si-N bond length is 1.6160 Å, which is much larger than the B-N sp^2 bonds (1.450 4 Å) of the pristine h-BN sheet, as given in Table 1. The calculated results agree with previously reported DFT calculation [27]. Similarly, the bond angle for Si-doped monolayer BN (B-N-Si) is measured to be 121°, which indicates a small increment of the bond angle in comparison to pristine band angle 120°. Thus, the increase in bond length and bond angle results from the corrugation induced by the radius of the Si atom (1.17 Å) bigger than the atomic radius of B (0.96 Å) atom.

3.2. Defect Formation Energy and Structural Stability. To examine the relative stability of Si atoms in pristine monolayer BN, we have calculated the formation energy (E_{form}) using the following equation [32, 33]:

$$E_{\text{form}} = E_{\text{tot}}(\text{Si, BN}) - E_{\text{tot}}(\text{BN}) - \sum_i n_i(\mu_{Si} - \mu_B), \quad (1)$$

where $E_{\text{tot}}(\text{Si, BN})$ and $E_{\text{tot}}(\text{BN})$ are the total energies of doped and pure monolayer BN, respectively. The integer n_i in equation (1) indicates the corresponding number of species that have been added to or removed from the supercell of monolayer BN, and μ_{Si} and μ_B are the chemical potentials of Si and B atoms, respectively. The calculated defect formation energy is employing the above equation (1) to be 4.83 eV and 1.71 eV for boron-rich and nitrogen-rich growth conditions, respectively. Our calculated results for boron-rich BN growth condition is closer to recently reported 4.86 eV, the formation energy Si-doping on BN for neutral defect [34]. Especially, our calculated formation energy for nitrogen-rich growth conditions is relatively small (1.71 eV). Thus, relatively small values of formation energy reveal that relative stability of Si impurities in monolayer BN and the doped Si atoms are closely bonded with neighboring B and N atoms of the mother compounds for nitrogen-rich BN growth condition than B-rich BN growth condition.

3.3. Electronic Properties Pure and Si-Doped Monolayer BN

3.3.1. Total Density of States and Partial Density of States. For a complete understanding of electronic states and individual contribution of atomic orbitals, we have plotted the total density of states (TDOS) and corresponding partial density of state (PDOS). As shown in Figure 2(a), the Fermi level of pristine monolayer BN is found at the middle of the valence band and conduction band. In addition, the spin-up state and spin-down state are symmetric, which confirm the semiconductor and nonmagnetic properties, respectively. However, in the presence of Si dopant, there are some additional localized impurity states seen in the spin-up state (Figure 2(b)) but not on the spin-down state. Moreover, symmetry in spin-up and spin-down TDOS are broken for the doped case. Furthermore, as impurity concentration increases, the defect states are broadening, as shown in Figures 2(b) and 2(c), which indicates the possibility of controlling the bandgap by manipulating the concentration of Si dopant.

Besides this, to get a clear understanding of which orbital is more contributing to the electronic properties, the partial density of states (PDOS) for the pure and single Si-doped BN was plotted. As shown in Figure 3(a), the major contributions for the state in the vicinity of Fermi level drive from nitrogen p orbital followed by boron p orbital for pure BN.

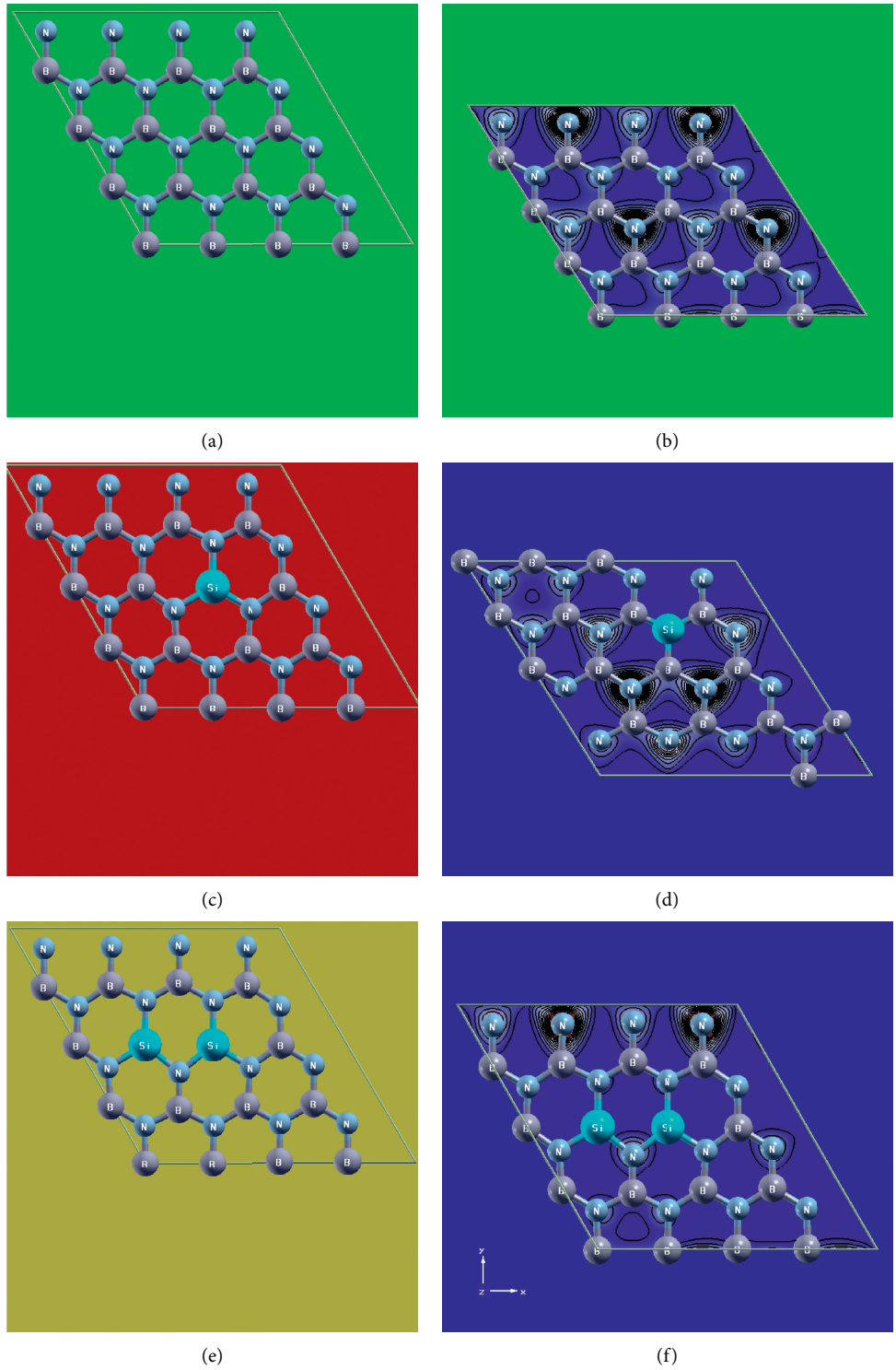

Figure 1: Optimized geometry of a $4 \times 4 \times 1$ BN supercell doped with single and two Si atoms and its isosurface plot of charge density. (a)-(b) Pure. (c)-(d) Single Si-doped BN. (e)-(f) Two Si-doped BN.

Table 1: The calculated B(Si)-N bond length, B(Si)-N-B(Si) bond angle, the calculated lattice constant (Cal.latt.const.), and the experimental lattice constant (Exp.latt.const.) of pure and silicon-doped monolayer boron nitride (BN).

System	B(Si)-N bond length in (Å)	N-B(Si)-N bond angle	Cal.latt.const. (Å)	Exp. bond length and latt.const.
Pure BN supercell	1.450 4	120 .00	2.512	1.446 Å [17] and 2.503 8 Å [31]
Single Si-doped supercell	1.616 0	121.78	2.582	

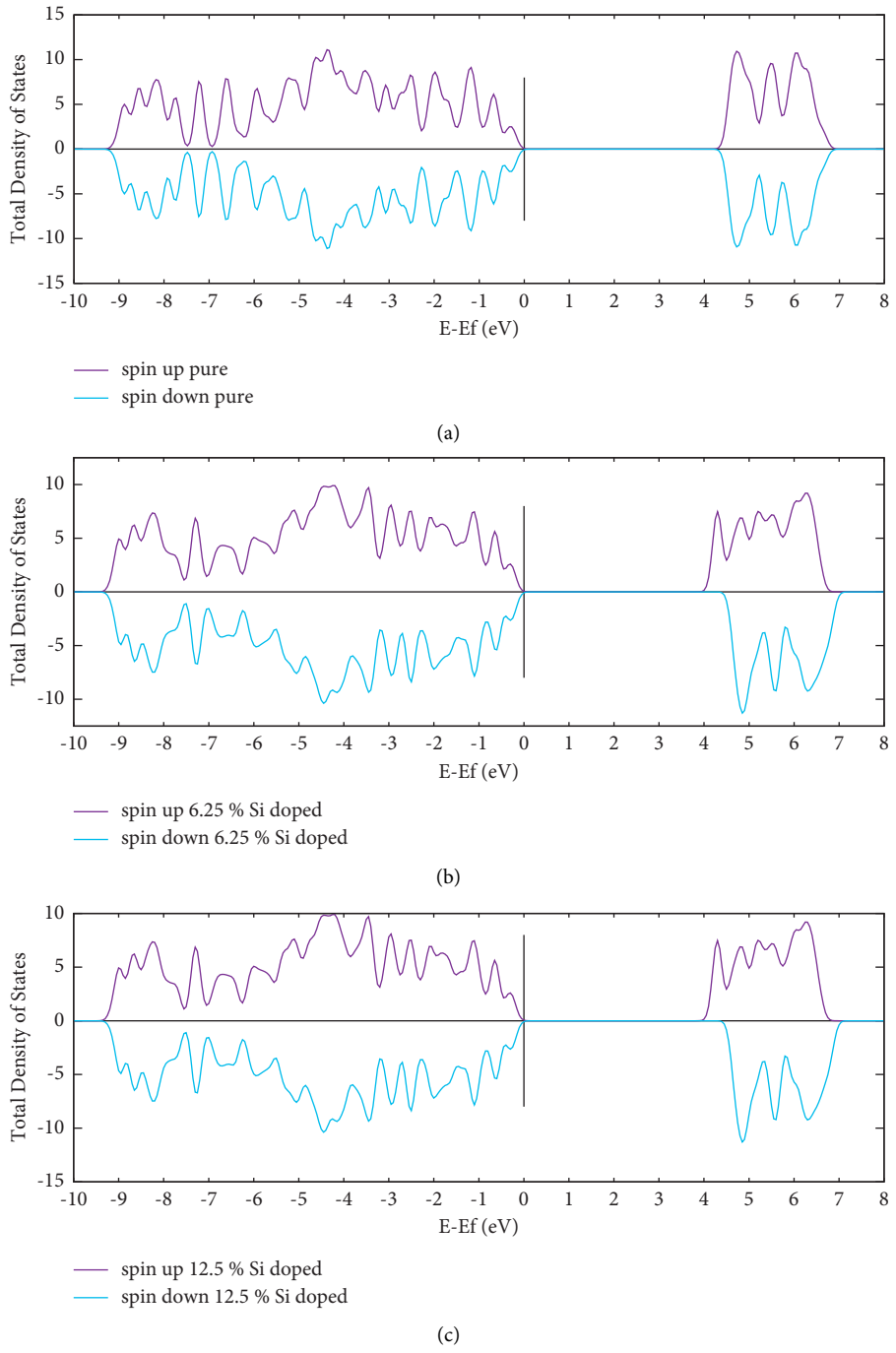

Figure 2: Calculated density of state for $4 \times 4 \times 1$ monolayer BN. (a) Pure. (b) 6.25% of silicon-doped BN. (c) 12.5% of silicon-doped BN. The blue-violet and blue lines represent the spin-up and spin-down components, respectively. The zero-energy represents the Fermi level.

However, for a single Si-doped BN, the main contribution in the vicinity of Fermi level is derived from silicon 3-p orbital electrons, as shown in Figure 1(b).

3.4. Band Structure of Pure and Silicon-Doped Monolayer Boron Nitride. To understand the nature of bandgap as well as the effect of Si-doping on energy band structure, the energy band structures were plotted for pure and single Si-doped in $4 \times 4 \times 1$ monolayer BN supercells. As shown in Figure 4(a), the valence band maximum (VBM) and conduction band minimum (CBM) are located at K-high symmetry points of 2D hexagonal BZ for the pure and doped system, indicating that the type of the bandgap is direct in nature. On the other hand, in Si-doped monolayer BN, the Fermi energy moves up to CBM, which suggests that in the Si-doped system, the carriers are more likely electrons (N-type of conductivity) and some localized states are formed. The isosurface charge plot shown in Figure 1(c) confirms this. Our result agrees with other latest findings [35]. In

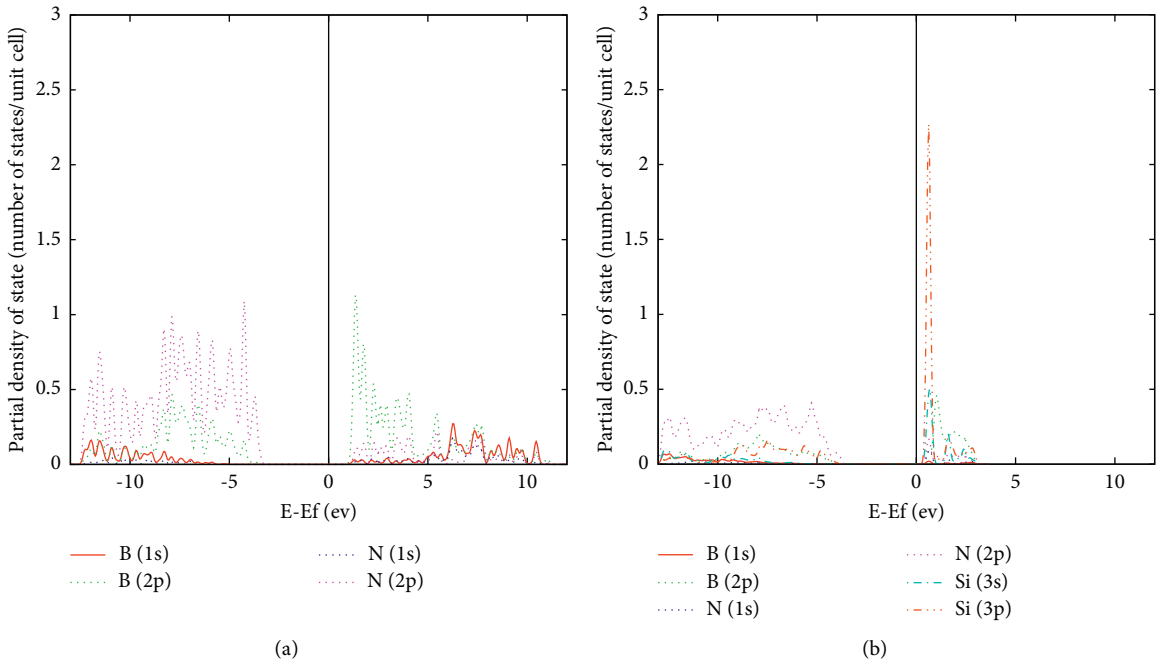

FIGURE 3: The calculated partial density of state (PDOS). (a) Pure monolayer BN. (b) Single Si-doped monolayer BN. The zero-energy represents the Fermi level.

addition, spin degeneracy in upstate and downstate is broken, as shown in Figures 4(c) and 4(d). The magnitude of the gap is found to be 4.4 eV, which is in good agreement with the previously reported theoretical bandgap of 4.4 eV [26] and less than the previously reported experimental optical band gap of 5.5 eV [17]. This is due to known limitations of DFT calculation like LDA and GGA overestimate the lattice parameters and underestimate the bandgap.

3.5. Effect of Si-Doping on Magnetic Properties of Pure Monolayer BN. To understand how the state is distributed, the total spin-polarized density of states (DOS) for pure and single Si-doped monolayer BN was plotted. As shown in Figure 2(a), the nature of DOS for up and down spin channels is symmetric for the pure MLBN system; thus, symmetric behavior of up and down spin channels of DOS indicates that these materials bear paramagnetic (nonmagnetic) semiconductor nature. As given in Table 2, the calculated total magnetic moment per supercell of pure monolayer BN is $\mu_m = 0\mu_B$. However, for single and two Si-doped monolayers BN, the total magnetic moment per supercell is $1.0\mu_B$ and $2.0\mu_B$, respectively. The calculated results are in good agreement with the recent DFT calculation [35]. Hence, the doped monolayer BN becomes ferromagnetic. The origin of magnetism seems to be an isolated Si atom that has the electron configuration [Ne] $(3s^2 3p^2)$ with one electron greater than the B atom electron configuration [He] $(2s^2 2p^1)$. Therefore, the substitution of Si with B introduces a single electron per dopant. Thus, the wave function electron overlaps with the nearest neighbor nitrogen p-orbitals and boron p-orbitals and the phenomenon of spin splitting happened.

3.6. Magnetic Interaction in Silicon-Doped Monolayer Boron Nitride. The magnetic interaction between Si atoms in doped BN is studied by calculating the magnetic energy (ΔE), the total energy difference of ferromagnetic state E_{Tot} (FM), and antiferromagnetic state E_{Tot} (AFM) at the same impurity separation using the relation [32, 33]

$$\triangle E = E_{\text{FM}} - E_{\text{AFM}}, \tag{2}$$

where E_{FM} and E_{AFM} are the total energies of the supercell in ferromagnetic (FM) and antiferromagnetic (AFM) states, respectively. Using the result in Table 2, the calculated $\triangle E$ is found to be −0.017 882 81 Ry. Thus, our calculated results show that the FM phase is more stable than AFM for the nearest neighbor impurity configuration.

3.7. Ferromagnetic Transition Temperature in Si-Doped Monolayer BN. The ferromagnetic transition temperature (T_c) below which the material maintains spontaneous magnetization is the most decisive parameter to characterize magnetic materials. By mapping the Heisenberg Hamiltonian together with the mean-field approximation, we have calculated T_C for 12.5% Si-doped monolayer BN using relation [32, 33]

$$\frac{3}{2}K_B T_c = -\frac{\triangle E}{N_{\text{imp}}}, \tag{3}$$

where N_{imp} is the number of impurities of silicon doped in super cell and K_B is the Boltzmann constant. Using the value of $\triangle E$ in Table 2, the number of silicon doped in monolayer BN is $N = 2$.

But, it is well known that the magnetic ordering in the doped system is strongly influenced by percolation. Thus, the

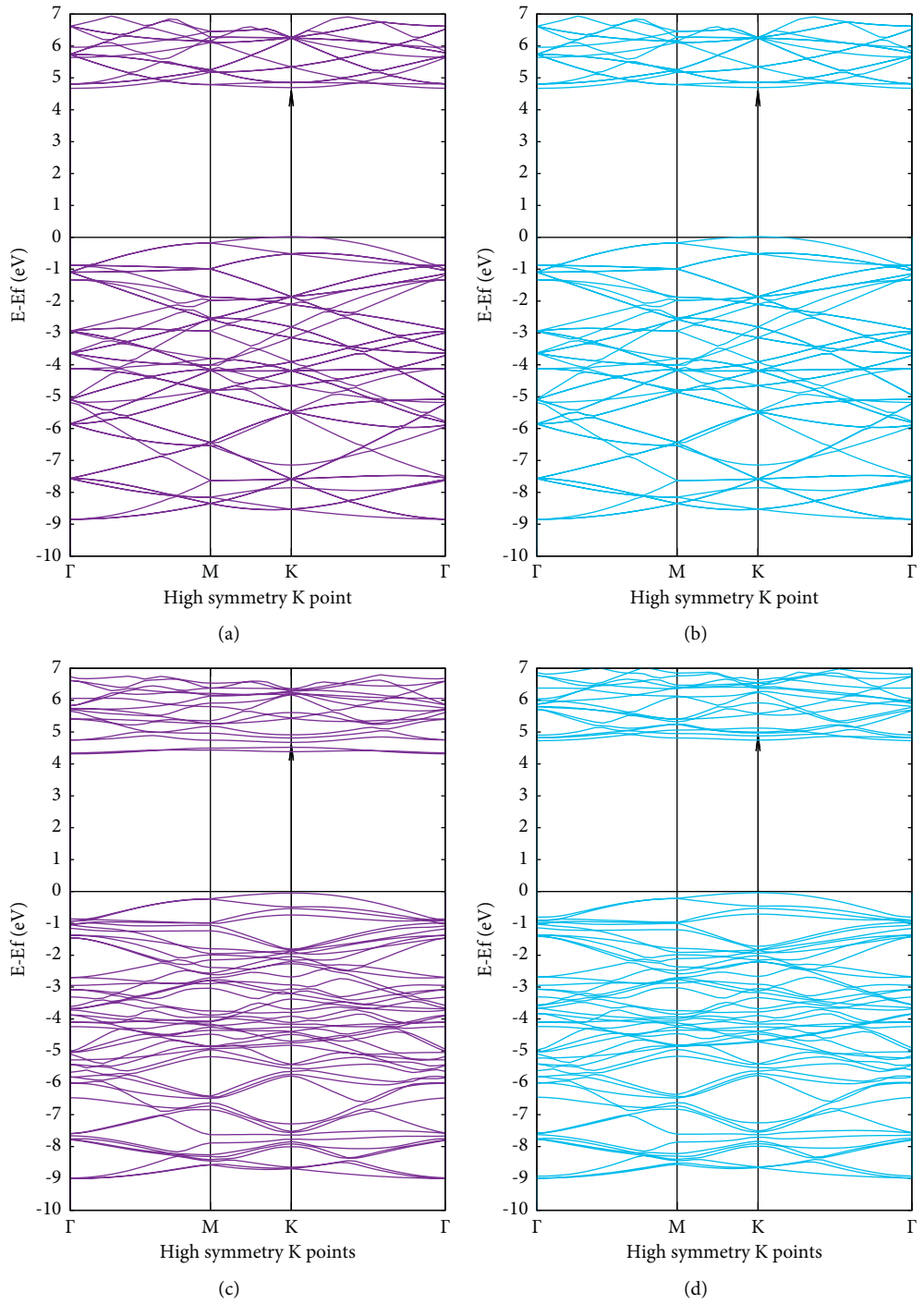

Figure 4: Calculated band structures of $4 \times 4 \times 1$ monolayer BN supercell. (a)-(b) Pure. (c)-(d) Single Si-doped. The blue-violet and blue lines represent the spin-up and spin-down components, respectively, and zero-energy represents the Fermi level.

Table 2: The calculated magnetic energy ($\triangle E = E_{\mathrm{FM}} - E_{\mathrm{AF}}$) and magnetic moment ($\mu_B$) for silicon-doped monolayer boron nitride.

System	E_{FM} (eV)	E_{AFM} (eV)	ΔE (eV)	Energy gap (eV)	$\mu_m\,(\mu_B)$	Magnetic ground state
Pure supercell	—	—	—	4.4	0	PM
12.5% Si-doped BN supercell	−5853.6745871	—	—	4.0	1	FM
6.25% Si-doped BN supercell	−5891.8183895	−5891.5750814	−0.2433081134	3.8	2	FM

mean field approximation cannot capture this behavior and tends to overestimate T_c in these systems. Therefore, to overcome this, we made use of some empirical relations that connect the mean-field value critical temperature (T_c^{MFA}) with corrected critical temperature (T_c^{corr}) as $T_c^{\mathrm{corr}} = (0.506)\, T_c^{\mathrm{MFA}}$ [32, 33], where T_c^{corr} is the corrected critical temperature calculated using the Ising model for hexagonal lattice and T_c^{MFA} predicted the critical temperature using mean-field theory as given in equation (3). The calculated Tc using mean filed approximation for 12.5% Si-doped monolayer BN and the corresponding corrected values are to be 940 K and 476 K, respectively. Hence, our result reveals that Si-doped monolayer BN is a promising candidate for room-temperature 2D dilutes magnetic semiconductors for spintronics applications even at high temperatures.

4. Conclusion

In this study, we have investigated the structural, electronic, and magnetic properties of Si-doped monolayer using spin-polarized DFT. The substitution of the Si atom in the pure monolayer BN supercell affects its structural properties; the band length increases from 1.450 4 Å to 1.616 0 Å, the band angle 120°-121°, and the lattice constant increases from 2.512 Å to 2.582 Å. Moreover, we have shown that the substitution of the Si atom in the pristine graphene supercell turns the insulator of the pristine graphene into a relatively narrow gap semiconductor. It is found that Si-doped monolayer BN is ferromagnetic. The calculated Curie temperature using the mean-field approximation together with spin-polarized DFT is found to be 474 K, 12.5%. In light of our result, we suggest that Si monolayer BN is a good candidate for 2D magnetic semiconductors for spintronics applications.

Data Availability

The data used to support the findings of this study are available from the corresponding author upon request.

Conflicts of Interest

The authors declare that there are no conflicts of interest.

Acknowledgments

The authors acknowledge the Arba Minch University (GoV/AMU/TH3/CNS/Chem/03/2 013), Arba Minch, Ethiopia, for providing computational facilities and financial support.

References

[1] Q. Zhang, J. Yu, P. Ebert et al., "Tuning band gap and work function modulations in monolayer hBN (Cu) (111) heterostructures with Moiré patterns," *ACS Nano*, vol. 12, no. 9, pp. 9355–9362, 2018.

[2] Y. Shi, C. Hamsen, X. Jia et al., Synthesis of few-layer hexagonal boron nitride thin film by chemical vapor deposition," *Nano Letters*, vol. 10, no. 1-12, pp. 4134–4139, 2010.

[3] Y. Tian, Bo Xu, D. Yu et al., "Ultrahard nano twinned cubic boron nitride," *Nature*, vol. 10, no. 493, p. 385, 2013.

[4] N. Miyata, K. Moriki, O. Mishima, M. Fujisawa, and T. Hattori, "Optical constants of cubic boron nitride," *Physical Review B: Condensed Matter*, vol. 40, no. 12028, p. 385, 1989.

[5] J. Y. J. Li and X. Zhao, "Semihydrogenated bn sheet: a promising visible-light driven photocatalyst for water splitting," *J. Scientific Reports*, vol. 3, no. 1858, p. 385, 2013.

[6] G. Kern, G. Kresse, and J. Hafner, "Ab initio calculation of the lattice dynamics and phase diagram of boron nitride," *Physical Review B*, vol. 59, no. 13, Article ID 8551, 1999.

[7] J. Wang, F. Ma, and M. Sun, "Graphene, hexagonal boron nitride, and their heterostructures: properties and applications," *RSC Advances*, vol. 7, no. 27, pp. 16801–16822, 2017.

[8] C. Pan, J. Zhang, K. Kou, Yu Zhang, and G. Wu, "Investigation of the through-plane thermal conductivity of polymer composites with in-plane oriented hexagonal boron nitride," *International Journal of Heat and Mass Transfer*, vol. 120, pp. 1–8, 2018.

[9] L. Bourgeois, Y. Bando, and T. Sato, "Tubes of rhombohedral boron nitride," *Journal of Physics D: Applied Physics*, vol. 33, no. 15, p. 1902, 200.

[10] Y. Zhang, H. Sun, and C. Chen, "Structural deformation, strength, and instability of cubic BN compared to diamond: a first-principles study," *Physical Review B*, vol. 73, no. 14, Article ID 144115, 2006.

[11] B. Vishal, R. Singh, A. Chaturvedi et al., "Chemically stabilized epitaxial wurtzite-BN thin film," *Superlattices and Microstructures*, vol. 115, pp. 197–203, 2018.

[12] K. S. Schedin, D. Novoselov, S. Jiang, T. J. Khotkevich, S. V. Morozov, and A. K. Geim, "Two-dimensional atomic crystals," *Journal of Proceedings of the National Academy of Science of the USA*, vol. 102, no. 30, pp. 10451–10453, 2005.

[13] P. D. Meyer, J. C. Girit, and Ç. Ö. Zettl, "The two-dimensional phase of boron nitride: few-atomic-layer sheets and suspended membranes," *Applied Physics Letters*, vol. 92, no. 13, Article ID 133107, 2018.

[14] I. V. Lebedeva, A. V. Lebedev, A. M. Popov, and A. A. Knizhnik, "Comparison of performance of van der Waals-corrected exchange-correlation functionals for interlayer interaction in graphene and hexagonal boron nitride," *Computational Materials Science*, vol. 128, pp. 45–58, 2017.

[15] X. Liu, Y. Wen, Z. Chen et al., "Modulation of Dirac points and band-gaps in graphene via periodic fullerene adsorption," *AIP Advances*, vol. 3, 2013.

[16] Y. Kubota, W. K. Tsuda, and O. Taniguchi, "Deep ultraviolet light-emitting hexagonal boron nitride synthesized at atmospheric pressure," *Science*, vol. 317, no. 5840, pp. 932–934, 2007.

[17] J. Wua, B. Wanga, Y. Weia, R. Yangb, and M. Dresselhaus, "Mechanics and mechanically tunable band gap in single-layer hexagonal boron-nitride," *Materials Research Letters*, vol. 1, no. 4, pp. 200–206, 2013.

[18] B. Arnaud, S. Lebègue, P. Rabiller, and M. Alouani, "Huge ,Excitonic effects in layered hexagonal boron nitride," *Physical Review Letters*, vol. 96, no. 2, Article ID 026402, 2006.

[19] L. Song, L. Ci, H. Lu et al., "Large scale growth and characterization of atomic heptagonal nitride layers," *Nano Letters*, vol. 10, no. 8, pp. 3209–3215, 2010.

[20] Yi Wang, G. Chen, H. Weng et al., "Carbon-doped boron nitride nanosheets with adjustable band structure for efficient photocatalytic U (VI) reduction under visible light," *Chemical Engineering Journal*, vol. 410, Article ID 128280, 2021.

[21] S. N. Rashkeev, M. Legesse, H. Saidaoui, F. E. Mcllouhi, S. Ahzi, and F. H. Alharbi, "Towards control of band gap in two-dimensional hexagonal boron nitride by doping," in *Proceedings of the International Renewable and Sustainable Energy Conference (IRSEC)*, pp. 1–4, Agadir, Morocco, November 2019.

[22] Y.-jie Liu, Bo Gao, D. Xu, H.-mei Wang, and J.-xiang Zhao, "Theoretical study on Si-doped hexagonal boron nitride(h-BN) sheet:Electronic, magnetic properties, and reactivity," *Physics Letters A*, vol. 378, pp. 2989–2994, 2014.

[23] J. Zhou, Q. Wang, Q. Sun, and P. Jena, "Electronic and magnetic properties of a BN sheet decorated with hydrogen and fluorine," *Physical Review B*, vol. 81, no. 8, Article ID 085442, 2010.

[24] Y. Lu, Xu Zuo, M. Feng, and T. Zhou, "Magnetic anisotropy in the boron nitride monolayer doped by 3d transitional metal substitutes at boron-site," *Journal of Applied Physics*, vol. 113, no. 17, p. 17C304, 2013.

[25] W. Zhou, "Erratum: long-range frustration in a spin-glass model of the vertex-cover problem," *Physical Review Letters*, vol. 109, Article ID 206803, 2012.

[26] S. K. Gupta, H. He, D. Banyai, M. Si, R. Pandey, and S. P. Karna, "Effect of Si doping on the electronic properties of BN monolayer," *Nanoscale*, vol. 6, no. 10, pp. 5526–5531, 2014.

[27] H. Bu, M. Zhao, H. Zhang, X. Wang, Xi Yan, and Z. Wang, ""Isoelectronic doping of graphdiyne with boron and nitrogen: stable configurations and band gap modification," *The Journal of Physical Chemistry A*, vol. 116, no. 15, pp. 3934–3939, 2012.

[28] P. Giannozzi, O. Andreussi, T. Brumme et al., "Advanced capabilities for materials modelling with Quantum ESPRESSO," *Journal of Physics: Condensed Matter*, vol. 29, Article ID 465901, 2017.

[29] J. Perdew, P. Kurth, S. Zupan, and P. Blaha, "Accurate density functional with correct formal properties: a step beyond the generalized gradient approximation," *Physical Review Letters*, vol. 82, no. 12, p. 2544, 1999.

[30] H. J. Monkhorst and J. D. Pack, "Special points for brillouin-zone integrations," *Physical Review Letters B*, vol. 13, Article ID 5188, 1976.

[31] W. Paszkowicz, J. Pelka, M. Knapp, T. Szyszko, and S. Podsiadlo, "Lattice parameters and anisotropic thermal expansion of hexagonal boron nitride in the 10–297.5 K temperature range," *Applied Physics A*, vol. 75, pp. 431–435, 2002.

[32] S. M. Hailemariam and A. E. Enna, "First principles investigation of structural, electronic, and room temperature ferromagnetism in V doped hexagonal pristine graphene," *AIP Advances*, vol. 11, no. 2, Article ID 025217, 2021.

[33] S. Mekonnen Hailemariam, "Electronic structure and room temperature of 2D dilute magnetic semiconductors in bilayer MoS2-doped Mn," *Advances in Condensed Matter Physics*, vol. 2020, pp. 1–8, Article ID 9635917, 2020.

[34] A. Monazam, M. Reza, U. Ludacka, H.-P. Komsa, and J. Kotakoski, "Substitutional Si impurities in monolayer hexagonal boron nitride," *Applied Physics Letters*, vol. 115, no. 7, Article ID 071604, 2019.

[35] R. E. Mapasha, M. P. Molepo, R. C. Andrew, and N. Chetty, "Defect charge states in Si doped hexagonal boron-nitride monolayer," *Journal of Physics: Condensed Matter*, vol. 28, no. 5, Article ID 055501, 2016.